FirstPage

Pure Spin Current Injection in Hydrogenated Graphene Structures

Reinaldo Zapata-Peña[1], Bernardo S. Mendoza[1], Anatoli I. Shkrebtii[2]

[1]*Centro de Investigaciones en Óptica, León, Guanajuato 37150, México and*

[2]*University of Ontario, Institute of Technology, Oshawa, ON, L1H 7L7, Canada*

(Dated: July 13, 2017)

perro

I. INTRODUCTION

sec:introduction

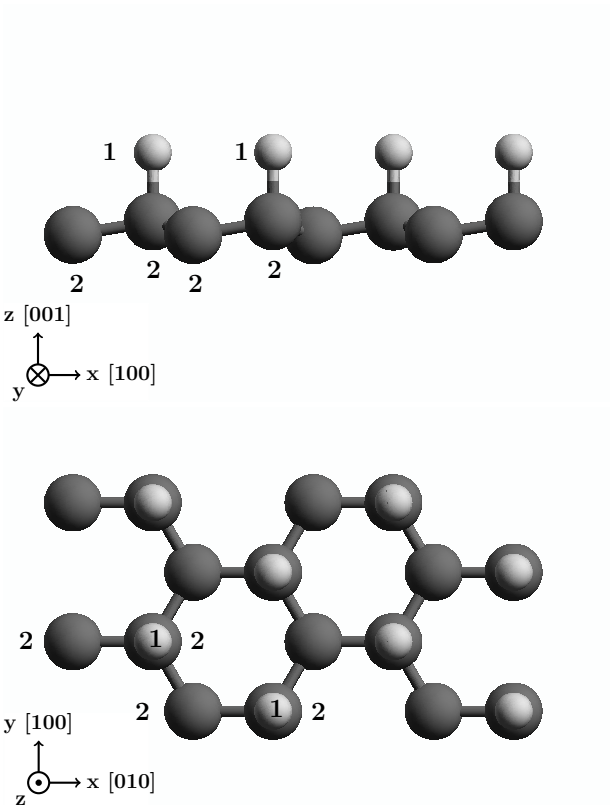

FIG. 1. Up structure fig:up-struc

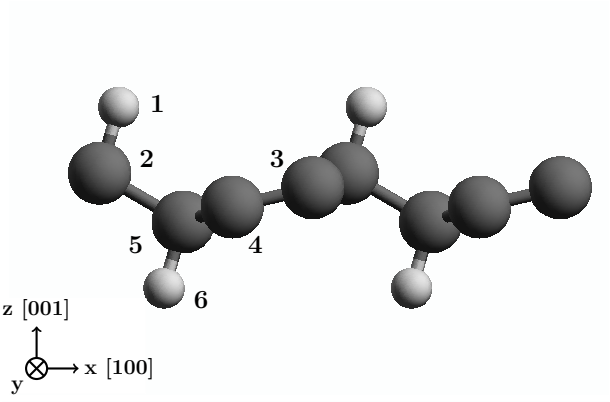

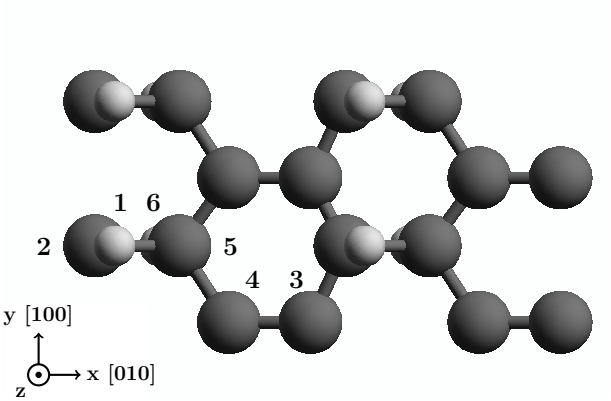

FIG. 2. Alt structure fig:alt-struc

Spintronics is an emerging research field of electronics in which the manipulation and transport of spin of electrons in a solid state media plays the determining role adding a new degree of freedom to the conventional charge manipulation.[1,2] At present there is an increasing interest in attain the same level of control over the transport of spin at micro or nano scales as has been done for the flow of charge in typical electronic devices.[3] Some semiconductor spintronics devices have been proposed[4–7] and some of them require spin polarized electrical current[8] or pure spin current (PSC). One of the difficulties to achieve the development of spin current and PSC semiconductor devices is the fact that the spin relaxation time in a semiconducting media is short disabling the spin transport and then resulting in a no observable spin current.[9] In PSCs there is no net motion of charge; spin-up electrons move in a given direction while spin-down electrons travel in the opposite one. This

phenomena can result from spin injection,[10] Hall Effects,[11] interference of two optical beams,[12,13] or one photon absorption of linearly polarized light[14] and has been observed in gallium arsenide (GaAs),[15,16] aluminum-gallium arsenide (AlGaAs),[16] and Co_2FeSi.[17]

Graphene, an allotrope of carbon with hexagonal 2D lattice structure presents properties like fractional quantum Hall effect at room temperature, excellent thermal transport properties, excellent conductivity[18] and strength[19–22] being then a perfect platform to be used in two-dimensions electronic systems; however most electronic applications are disabled by the absence of a semiconducting gap. Recent studies demonstrate that the band gap of graphene can be opened by applying an electric field,[23] reducing the surface area,[24] or applying uniaxial strain.[25] Another possibility to open the gap is by doping; this has been successfully achieved using nitrogen,[26] boron-nitrogen,[27] silicon,[28] noble-metals,[29] and hydrogen.[30–32] Depending on the percentage of hydrogenation and spatial configurations of hydrogen-carbon bonds, hydrogenated graphene can result in different spatial configurations. In this paper we present two 50% hydrogenated graphene noncentrosymmetric structures both presenting a discernible band gap: the *up* structure, shown in Fig. 1, has hydrogen atoms bonded to the carbon layer only in the upper side of the structure while the *alt* structure, shown in Fig. 2, has hydrogen alternating in the upper and bottom sides of the carbon slab.[33]

Using those structures we address a theoretical study of the spin velocity injection (SVI) by one-photon absorption of linearly polarized light. Because we have 2D structures we made the analysis for tow cases. The first is fixing the spin of the electrons along the z Cartesian direction with the velocity directed on the surface of the structure in the xy plane. The second is fixing the spin velocity in the x or y direction and the spin directed in xyz. The SVI is an optical effect that quantifies the velocity at which a PSC moves along the Cartesian direction a with the spin of electron polarized along the Cartesian direction b. One photon absorption of linearly polarized light can promote a distribution of electrons in $\mathbf{k}$ space regardless the symmetry of the material resulting in a null electrical current. Then, the electrons excited to the conduction bands at opposite $\mathbf{k}$ points will result in opposite spin polarizations producing no net spin injection.[14] If the crystalline structure of the material is noncentrosymmetric the spin polarization injected at a given $\mathbf{k}$ point could not vanish[34,35] and then, since the velocities of electrons at opposite $\mathbf{k}$ points are opposite, a pure spin current will be produced. Since the structures presented here are noncentrosymmetric, they are good candidates in which this effect can be induced.

This paper is organized as follows. In Section II we present the theory and formulas that describe PSC and SVI. In Section III we describe the details of calculations and the corresponding SVI spectra for the *up* and *alt* structures. Finally, we present our conclusions in Section IV.

II. THEORY

sec:theory

In this section, we report a summary of the theory that involves the PSC phenomena from which rises the SVI treated in this paper.

In PSCs there is no net motion of electrical charge and spin-up electrons move in a given direction while spin-down electrons travel in the opposite one. This effect can result from one photon absorption of linearly polarized light by a semiconductor, with filled valence bands and empty conduction bands, illuminated by light with photon energy larger than the energy gap. Using a single continuous linearly polarized laser beam, it is possible to promote electrons in $\mathbf{k}$ space regardless the symmetry of the system resulting in a net current equal to zero. If the phenomena is produced in a noncentrosymmetric semiconducting media, the electrons promoted to the conduction bands at opposite $\mathbf{k}$ points can produce a net spin polarization different to zero[34], resulting in a PSC because the velocity of electrons at opposite $\mathbf{k}$ points are in opposite directions.

The operator that describes the electronic

PSC is written as

$$\hat{K}^{\rm ab} = \frac{1}{2}\left(\hat{v}^{\rm a}\hat{S}^{\rm b} + \hat{S}^{\rm b}\hat{v}^{\rm a}\right), \tag{1}$$

where $\hat{\mathbf{v}} = [\hat{\mathbf{r}}, \hat{H}_0]/i\hbar$ is the velocity operator, with $\hat{\mathbf{r}}$ the position operator, $\hat{H}_0$ the unperturbed ground state Hamiltonian, and the Roman superscripts indicate Cartesian coordinates. To obtain the expectation value of $\hat{K}^{\rm ab}$, we use the length gauge for the perturbing Hamiltonian, written as

$$\hat{H}_{\rm p} = -e\hat{\mathbf{r}}\cdot\mathbf{E}(t), \tag{2}$$

where the electric field of the applied laser is given by

$$\mathbf{E}(t) = \mathbf{E}(\omega)e^{-i\omega t} + \mathbf{E}^*(\omega)e^{i\omega t}. \tag{3}$$

In order to calculate the response of the system to $\mathbf{E}(t)$, one needs to take into account the excited coherent superposition of the spin-splited conduction bands inherent to the noncentrosymmetric semiconductors considered in this work. To include the coherences, we follow Ref. 36 and use a multiple scale approach that solves the equation of motion for the single particle density matrix $\rho_{mn}(\mathbf{k};t)$, leading to

$$\frac{\partial\rho_{cc'}(\mathbf{k})}{\partial t} = \frac{e^2E^{\rm a}(\omega)E^{\rm b*}(\omega)}{i\hbar^2}\sum_v r^{\rm a}_{cv}(\mathbf{k})r^{\rm b}_{vc'}(\mathbf{k}) \times\left(\frac{1}{\omega-\omega_{c'v}(\mathbf{k})-i\epsilon} - \frac{1}{\omega-\omega_{cv}(\mathbf{k})+i\epsilon}\right), \tag{4}$$

where we assumed that the conduction bands c and c' are quasidegenerate states and we take $\epsilon\to 0$ at the end of the calculation. The spin-splitting of the valence (v) bands is very small, and is neglected throughout this work.[?] The matriz elements of any operator $\mathcal{O}$ are given by $\mathcal{O}_{nm}(\mathbf{k}) = \langle n\mathbf{k}|\hat{\mathcal{O}}|m\mathbf{k}\rangle$, where $H_0|n\mathbf{k}\rangle = \hbar\omega_n(\mathbf{k})|n\mathbf{k}\rangle$ with $\hbar\omega_n(\mathbf{k})$ the energy of the electronic band n at point $\mathbf{k}$ in the irreducible Brillouin zone (IBZ), $|n\mathbf{k}\rangle$ is the Bloch state, and $\omega_{nm}(\mathbf{k}) = \omega_n(\mathbf{k}) - \omega_m(\mathbf{k})$. Using $\mathcal{O} = {\rm Tr}(\hat{\rho}\hat{\mathcal{O}})$ for the expectation value of an observable $\mathcal{O}$, where Tr denotes the trace, we obtain

$$\mathcal{O} = \int\frac{d^3k}{8\pi^3}\sum_{cc'}\rho_{cc'}(\mathbf{k})\mathcal{O}_{c'c}(\mathbf{k}), \tag{5}$$

where we used the closure relationship $\sum_n |n\mathbf{k}\rangle\langle n\mathbf{k}| = 1$, where $n = v, c$, and the fact that $\rho_{vn}(\mathbf{k}) = \rho_{nv}(\mathbf{k}) = 0$ for $n = c, c'$. Therefore, using Eqs. (4) and (5), the rate of change of $\mathcal{O}$, $\dot{\mathcal{O}} = {\rm Tr}\left(\frac{\partial\hat{\rho}}{\partial t}\hat{\mathcal{O}}\right)$, is given by

$$\dot{\mathcal{O}} = \frac{e^2}{i\hbar^2}\int\frac{d^3k}{8\pi^3}{\sum_{cc'}}'\mathcal{O}_{c'c}(\mathbf{k})r^{\rm a}_{cv}(\mathbf{k})r^{\rm b}_{vc'}(\mathbf{k})\times \left(\frac{1}{\omega-\omega_{c'v}(\mathbf{k})-i\epsilon} - \frac{1}{\omega-\omega_{cv}(\mathbf{k})+i\epsilon}\right)E^{\rm a}(\omega)E^{\rm b*}(\omega). \tag{6}$$

Replacing $\hat{\mathcal{O}}\to\hat{K}^{\rm ab}$, in above expression, one can show that

$$\dot{K}^{\rm ab}(\omega) = \mu^{\rm abcd}(\omega)E^{\rm c}(\omega)E^{\rm d*}(\omega), \tag{7}$$

where repeated cartesian are summed, and

$$\mu^{\rm abcd}(\omega) = \frac{\pi e^2}{\hbar^2}\int\frac{d^3k}{8\pi^3}{\sum_{vcc'}}'\delta(\omega-\omega_{cv}(\mathbf{k}) \times{\rm Re}\left[K^{\rm ab}_{cc'}(\mathbf{k})\left(r^{\rm c}_{vc'}(\mathbf{k})r^{\rm d}_{cv}(\mathbf{k}) + (c\leftrightarrow d)\right)\right], \tag{8}$$

is the pseudotensor that describes the rate of change of the PSC process in semiconductors. To derive above we used $K^{\rm ab}_{nm}(-\mathbf{k}) = K^{\rm ab*}_{nm}(\mathbf{k})$. that follows from time-reversal invariance. The prime $'$ in the sum means that c and c' are quasi degenerate states and the sum only covers these states. Since $\mu^{\rm abcd}(\omega)$ is real we have that $\mu^{\rm abcd}(\omega) = \mu^{\rm abdc}(\omega)$. We remark that Eq. (8) is the same as Eq. (3) of Bhat et al.[14] obtained by using the semiconductor optical Bloch equations. Using the closure relation,

$$K^{\rm ab}_{cc'}(\mathbf{k}) = \frac{1}{2}\sum_{l=v,c}\left(v^{\rm a}_{cl}(\mathbf{k})S^{\rm b}_{lc'}(\mathbf{k}) + S^{\rm b}_{cl}(\mathbf{k})v^{\rm a}_{lc'}(\mathbf{k})\right). \tag{9}$$

Now, we define the spin velocity injection (SVI) as

$$\mathcal{V}^{\rm ab}(\omega) \equiv \frac{\dot{K}^{\rm ab}(\omega)}{(\hbar/2)\dot{n}(\omega)}, \tag{10}$$

that gives the velocity, along the direction a, at which the spin moves polarized along the direction b. The carrier injection rate $\dot{n}(\omega)$ is written as,[36]

$$\dot{n}(\omega) = \xi^{\rm ab}(\omega)E^c(\omega)E^{d*}(\omega), \tag{11}$$

where the tensor

$$\xi^{\mathrm{ab}}(\omega) = \frac{2\pi e^2}{\hbar^2}\int \frac{d^3k}{8\pi^3} \times \sum_{vc} r^{\mathrm{a}}_{vc'}(\mathbf{k}) r^{\mathrm{b}}_{cv}(\mathbf{k})\delta(\omega - \omega_{cv}(\mathbf{k}),$$

is related to the imaginary part of the linear optical response tensor by $\mathrm{Im}[\epsilon^{\mathrm{ab}}(\omega)] = 2\pi\epsilon_0\hbar\xi^{\mathrm{ab}}(\omega)$.

The function $\mathcal{V}^{\mathrm{ab}}(\omega)$ allow us to quantify two very important aspects of PSC. On one hand, we can fix the spin direction along b, and calculate the resulting electron velocity. On the other hand, we can fix de velocity of the electron along b, and study the resulting direction along which the spin is polarized. To this end, the added advantage of 2D structures, besides choosing them noncentrosymmetric, is that we can use an incoming linearly polarized beam of light at normal incidence, and use the direction of the polarized electric field to control $\mathcal{V}^{\mathrm{ab}}(\omega)$. Indeed, writing $\mathbf{E}(\omega) = E_0(\omega)(\cos\alpha\,\hat{\mathbf{x}} + \sin\alpha\,\hat{\mathbf{y}})$ where α is the polarization angle, we obtain from Eq. (10) that

$$\mathcal{V}^{\mathrm{ab}}(\omega,\alpha) = \frac{2}{\hbar\xi(\omega)}\left(\mu^{\mathrm{abxx}}(\omega)\cos^2\alpha + \mu^{\mathrm{abyy}}(\omega)\sin^2\alpha + \mu^{\mathrm{abxy}}(\omega)\sin 2\alpha\right) \quad (12)$$

as for the structures chosen in this article, $\xi^{\mathrm{xx}}(\omega) = \xi^{\mathrm{yy}}(\omega) \equiv \xi(\omega)$, and $\xi^{\mathrm{xy}}(\omega) = 0$. Now, we formalize our two options for $\mathcal{V}^{\mathrm{ab}}$.

A. Fixing spin

Analyzing the SVI, Eq. (12), we define the magnitude of the electron's in plane velocity with it's spin polarized along the b direction as

$$\mathcal{V}_{\sigma^{\mathrm{b}}}(\omega,\alpha) \equiv \sqrt{[\mathcal{V}^{\mathrm{xb}}(\omega,\alpha)]^2 + [\mathcal{V}^{\mathrm{yb}}(\omega,\alpha)]^2}\,, \quad (13)$$

and define the angle at which the velocity is directed on the xy plane as

$$\gamma_{\sigma^{\mathrm{b}}}(\omega,\alpha) = \tan^{-1}\left(\frac{\mathcal{V}^{\mathrm{yb}}(\omega,\alpha)}{\mathcal{V}^{\mathrm{xb}}(\omega,\alpha)}\right). \quad (14)$$

We also define two special angles

$$\gamma^{\parallel}_{\sigma^{\mathrm{b}}}(\omega,\alpha) = \alpha, \quad (15)$$

and

$$\gamma^{\perp}_{\sigma\mathrm{b}}(\omega,\alpha) = \alpha \pm 90^{\circ}, \quad (16)$$

corresponding to the electron velocity being parallel or perpendicular the incoming polarization, respectively. The subscript σ^{b} denotes the spin along b.

B. Fixing velocity.

Fixing the calculated velocity along $\mathrm{a} = x$ or $\mathrm{a} = y$ we define it's corresponding magnitude as

$$\mathcal{V}_{\mathrm{a}}(\omega,\alpha) \equiv \sqrt{[\mathcal{V}^{\mathrm{ax}}(\omega,\alpha)]^2 + [\mathcal{V}^{\mathrm{ay}}(\omega,\alpha)]^2 + [\mathcal{V}^{\mathrm{az}}(\omega,\alpha)]^2}, \quad (17)$$

from where we see that the spin would be oriented in the xyz system's coordinates according to a polar angle

$$\theta_{\mathrm{a}}(\omega,\alpha) = \cos^{-1}\left(\frac{\mathcal{V}^{\mathrm{az}}(\omega,\alpha)}{\mathcal{V}_{\mathrm{a}}(\omega,\alpha)}\right), \quad 0 \leq \theta \leq \pi, \quad (18)$$

and an azimuthal angle

$$\varphi_{\mathrm{a}}(\omega,\alpha) = \tan^{-1}\left(\frac{\mathcal{V}^{\mathrm{ay}}(\omega,\alpha)}{\mathcal{V}^{\mathrm{ax}}(\omega,\alpha)}\right), \quad 0 \leq \varphi \leq 2\pi. \quad (19)$$

III. RESULTS

We preset the results for and $\mathcal{V}_{\sigma^{\mathrm{b}}}(\omega,\alpha)$ and $\mathcal{V}_{\mathrm{a}}(\omega,\alpha)$ for the $C_{16}H_8$-up and $C_{16}H_8$-alt structures being both noncentrosymmetric semi-infinite 2D carbon systems with 50% hydrogenation in different arrangements. We recall that

Layer No.	Atom type	Position [Å] x	y	z
1	H	-0.61516	-1.77416	0.73196
1	H	0.61518	0.35514	0.73175
2	C	-0.61516	-1.77264	-0.49138
2	C	-0.61516	-0.35600	-0.72316
2	C	0.61516	0.35763	-0.49087

TABLE I. Unit cell of *up* structure. Layer division, atom types and positions for the *up* structure. The structure unit cell was divided in two layers corresponding to hydrogen and carbon atoms.The corresponding layer atom position is depicted in Fig. 1 with the corresponding number of layer. tab:up-unitcell

Layer No.	Atom type	Position [Å] x	y	z
1	H	-0.61516	-1.42140	1.47237
2	C	-0.61516	-1.73300	0.39631
3	C	0.61516	1.73300	0.15807
4	C	0.61516	0.42201	-0.15814
5	C	-0.61516	-0.37396	-0.39632
6	H	-0.61516	-0.68566	-1.47237

TABLE II. Unit cell of *alt* structure. Layer division, atom types and positions for the *alt* structure. The structure unit cell was divided in six layers corresponding each one to atoms in different z positions. The corresponding layer atom position is depicted in Fig. 2 with the corresponding number of layer. tab:alt-unitcell

the *up* structure has hydrogen atoms only on the upper side of the carbon sheet while the *alt* structure has alternating hydrogen atoms on the upper and bottom sides. Also we take the hexagonal carbon lattice to be on the xy plane for both structures, and the carbon-hydrogen bonds on the perpendicular xz plane, as depicted in Figs. 1 and 2. The coordinates for the *up* and *alt* unit cells of the structures are presented in Tables I and II.

We calculated the self-consistent ground state and the Kohn-Sham states using density functional theory in the local density approximation (DFT- LDA) with a planewave basis using the ABINIT code[37]. We used Hartwigsen-Goedecker-Hutter (HGH) relativistic separable dual-space Gaussian pseudopotentials[38] including the spin-orbit interaction needed to calculate $\mu^{\rm abcd}(\omega,\alpha)$ presented in Eq. (8). The convergence parameters for the calculations of our results corresponding to the *up* and *alt* structures are cutoff energies of 65 Ha and 40 Ha, resulting in LDA energy band gaps of 0.088 eV and 0.720 eV, respectively. The energy eigenvalues and matrix elements for the *up* and *alt* structures were calculated using 12802 $\mathbf{k}$ points and 14452 $\mathbf{k}$ points in the IBZ to integrate $\mu^{\rm abcd}(\omega)$ and $\xi^{\rm ab}(\omega)$ using the linearized analytic tetrahedron method (LATM).[39] We neglect the anomalous velocity term $\hbar(\boldsymbol{\sigma}\times\nabla V)/4m^2c^2$, where V is the crystal potential, in $\hat{\mathbf{v}}$ of Eq. (1), as this term is known to give small contribution to PSC.[14] Therefore, $[\hat{\mathbf{v}},\hat{\mathbf{S}}]=0$ and Eq. (1) reduces to $\hat{K}^{\rm ab}=\hat{v}^{\rm a}\hat{S}^{\rm b}=\hat{S}^{\rm b}\hat{v}^{\rm a}$.

A. SVI: Spin velocity injection

sec:res-spin_velocity

Using Eq. (12), we calculated $\mathcal{V}^{\rm ab}(\omega,\alpha)$ for the *up* and *alt* 2D structures and for CdSe and GaAs which are bulk systems; the results are presented in Fig. 3. The angle α presented in the response of each structure is that for which the response is maximized in each case. The most intense response corresponds to the *up* structure centered at 0.088 eV corresponding to the long-wavelength infrared radiation (LWIR) and reaching a $\mathcal{V}^{\rm yz}=87.2$ Km/s, which means the electrons moving along y (parallel to the surface) with the spin polarized along z (perpendicular to the surface), with a speed of 87.2 Km/s. For an

Structure	Kind of system	Pol. Ang.	Energy [eV]	$\mathcal{V}^{\rm ab}(\omega,\alpha)$ ab	[Km/s]
up	2D	40	0.088	yz	87.2
			1.938	yz	22.2
			1.972	yz	-29.7
alt	2D	145	0.720	yz	-40.2
			0.912	yz	-32.9
CdSe	bulk	90	0.906	zz	-26.9
GaAs	bulk	90	2.312	xx	-21.6

TABLE III. Comparison of the reported maxima values of $\mathcal{V}^{\rm ab}$ for the different structures and their corresponding polarization angle α and energy values of the incoming beam at which the maxima is obtained. tab:vab-str-comp

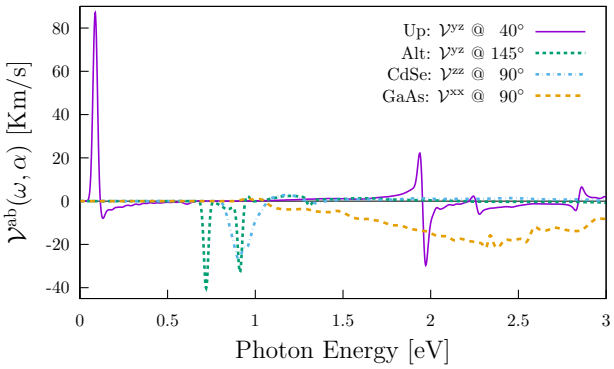

FIG. 3. Comparison of most intense responses of $\mathcal{V}^{ab}$ for 2D *alt* and *up*, and bulk CdSe and GaAs structures and their corresponding polarization angle α.

fig:vab-str-comp

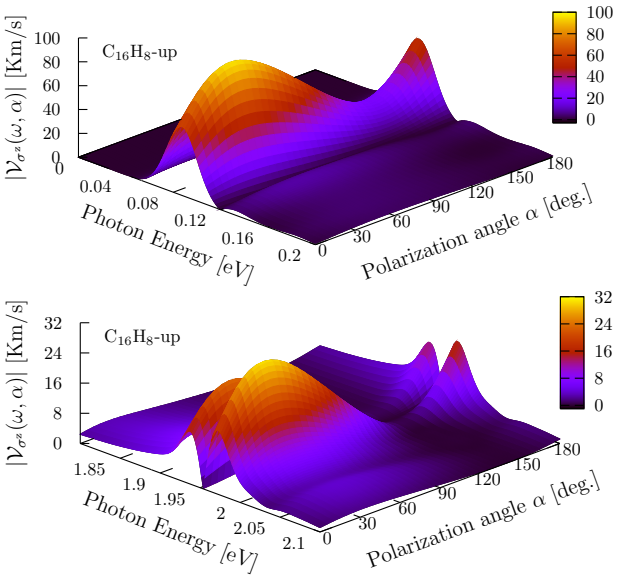

FIG. 4. $\mathcal{V}_{\sigma^z}(\omega,\alpha)$ response as a function of the photon energy and polarization angle α for the *up* structure for two energy ranges. The absolute maxima is located for an energy range from 0.08 eV to 0.10 eV, in the LWIR range, and two local maxima from 1.90 eV to 1.93 eV and from 1.96 eV to 2.0 eV, in the VIS range, all for polarization angles between 25° and 50°.

fig:up-vsz-3d

energy range from 0.66 eV to 3.0 eV, corresponding to energies of the Near Infrared (NIR) to visible radiation (VIS), all four systems have contributions of the same order of magnitude. For this energy range the *up* structure has two peaks centered at 1.938 eV and 1.972 eV reaching $\mathcal{V}^{yz} = 22.2$ Km/s and $\mathcal{V}^{yz} = -29.7$ Km/s and the *alt* structure has two peaks centered at 0.720 eV and 0.912 eV reaching $\mathcal{V}^{yz} = -40.2$ Km/s and $\mathcal{V}^{yz} = -32.9$ Km/s, respectively. Then, for the bulk structures we have that the CdSe has only one intense response centered at 0.906 eV reaching $\mathcal{V}^{zz} = -26.9$ Km/s, and the GaAs structure response reaches the maximum centered at 2.312 eV reaching $\mathcal{V}^{xx} = \mathcal{V}^{yy} = -21.6$ Km/s. In table III we present the comparison of these values for the 2D and bulk structures; a positive (negative) spin-velocity means that the velocity moves (anti-)parallel to the electric field. We remark that the 2D structures have resonances that give larger values for $\mathcal{V}^{ab}$ than the bulk crystals; in particular the *up* structure is ~ 5 times more intense.

B. Fixing spin

sec:res-fixspin

Using Eq. (13), we calculated $\mathcal{V}_{\sigma^b}(\omega,\alpha)$ and made the analysis for the case when the spin is fixed along z, i.e. directed perpendicularly to the surface of the *up* and *alt* structures. Also, using Eq. (14), we determined the angle $\gamma_b(\omega,\alpha)$ where the spin-velocity is directed along the surface of the each structure.

1. *up structure*

up:fs

We present in Fig. 4 $\mathcal{V}_{\sigma^z}(\omega,\alpha)$ for the two energy ranges of the *up* structure that give the highest values for $\mathcal{V}^{yz}$ shown in Fig. 3. We obtain that the zone where the maximum response is reached corresponds to a energy range of the incident beam from 0.084 eV to 0.093 eV, corresponding to the LWIR, and polarization angles α between 30° and 45°. Also, two local maxima are held for same α between 30° and 45°, but for an energy range between 1.90 eV and 2.05 eV, in the VIS range.

In the top panel of Fig. 5 we first analyze the response for $\hbar\omega = 0.088$ eV which gives the maximum as shown in Fig. 4 . We show $\mathcal{V}_{\sigma^z}(\omega,\alpha)$ as a function of α (left scale, black solid line). The absolute maximum is obtained when $\alpha = 40°$ resulting in a value of $\mathcal{V}_{\sigma^z}(\omega,\alpha) = 95.8$ Km/s, that according to Eq. (13) comes from $\mathcal{V}^{xz}(\omega,\alpha) = 39.8$ Km/s and $\mathcal{V}^{yz}(\omega,\alpha) = 87.2$ Km/s. In the same panel we present the corresponding velocity angle $\gamma_z(\omega,\alpha)$ (right scale, red dashed line),

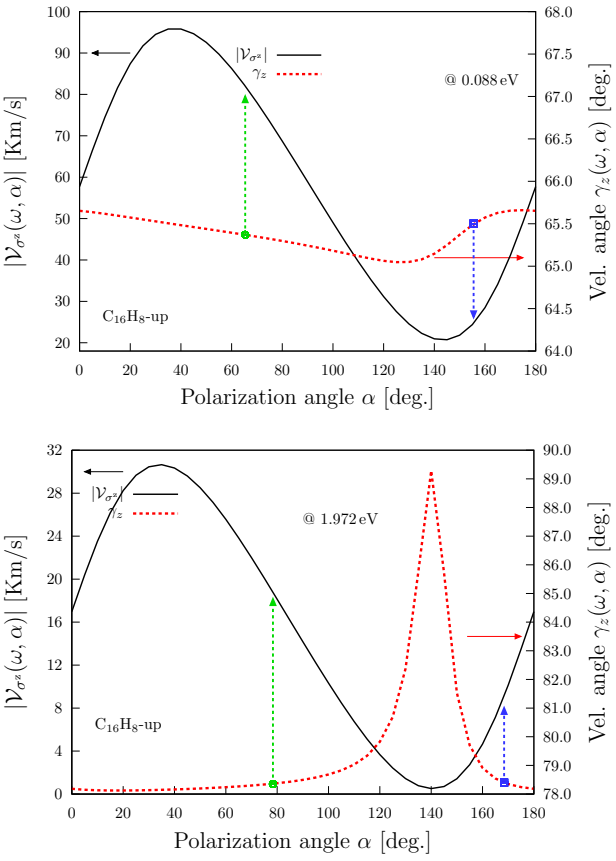

FIG. 5. For the *up* structure and fixing the energy to 0.088 eV (top panel) and 1.972 eV (lower panel), we show $\mathcal{V}_{\sigma^z}(\omega,\alpha)$ (left scale), the corresponding velocity angle $\gamma_z(\omega,\alpha)$ (right scale), the collinear (green arrow) and perpendicular (blue arrow) angles. `fig:up-vaz-rag`

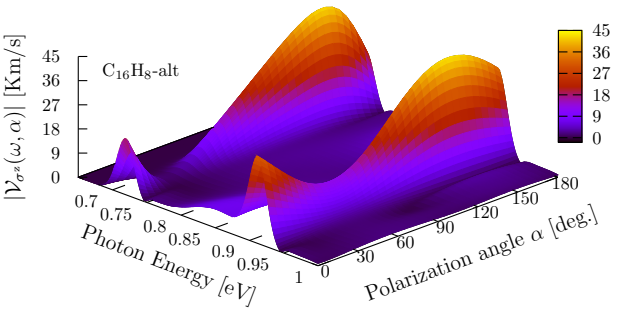

FIG. 6. $|\mathcal{V}_{\sigma^z}(\omega,\alpha)|$ response as a function of the photon energy and polarization angle α for the *alt* structure. The local and the absolute maxima are located in the energy ranges from 0.67 eV to 0.73 eV and from 0.90 eV to 0.93 eV, respectively, and both in the Near Infrared and for polarization angles between 120° and 150°. `fig:alt-3d-vsb`

that for the absolute maximum at $\alpha = 40°$ is $\gamma_z(\hbar\omega = 0.088\text{eV}, \alpha = 40°) = 65°$. This results means that at $\hbar\omega = 0.088$ eV and a polarization angle of the incoming electric field of $\alpha = 40°$ the electrons with a spin pointing along z move at angle of $\gamma_z(\hbar\omega = 0.088\text{eV}, \alpha = 40°) = 65°$ with respect to the x direction, with a maximum speed $\mathcal{V}_{\sigma^z}(\omega,\alpha)$ of 95.8 Km/s. Also, from Eq. (15) we find that $\gamma_z^{\parallel}(\omega,\alpha) = \alpha = 65.4°$, with $\mathcal{V}_{\sigma^z}(\omega,\alpha) = 82.3$ Km/s (see green arrow), and that from Eq. (16), $\gamma_z^{\perp}(\omega,\alpha) = \alpha - 90° = 65.5°$, gives $\alpha = 155.5°$, with $\mathcal{V}_{\sigma^z}(\omega,\alpha) = 24.8$ Km/s (see blue arrow); thus, for $\hbar\omega = 0.088$ eV, an $\alpha = 65.4°$ ($\alpha = 155.5°$) gives electrons with spin polarized along z moving parallel (perpendicular) to the incident electric field, with a speed of 82.3 (24.8) Km/s. We also find that for all values of α, $\gamma_z(\omega,\alpha) = 65.4° \pm 0.3°$, being almost constant, and 20 Km/s $< \mathcal{V}_{\sigma^z}(\omega,\alpha) <$ 95.8 Km/s.

In the bottom panel of Fig. 5, now we take $\hbar\omega = 1.972$ eV which is the local maximum shown in the bottom panel of Fig. 4. The local maximum is again at $\alpha = 40°$ with $\mathcal{V}_{\sigma^z}(\omega,\alpha) = 30.3$ Km/s and $\gamma_z(\omega,\alpha) = 78.2°$. In this case, $\alpha = \gamma_z^{\parallel}(\omega,\alpha) = 78.4°$ with $\mathcal{V}_{\sigma^z}(\omega,\alpha) =$ 18.8 Km/s (green circled box and arrow), and $\gamma_z^{\perp}(\omega,\alpha) = 78.5°$, for $\alpha = 168.5°$ (blue squared box and arrow). We find that the velocity angle is almost constant at $78.4° \pm 0.3°$ for $0° \leq \alpha \leq 100°$, and 1 Km/s $< \mathcal{V}_{\sigma^z}(\omega,\alpha) <$ 30.3 Km/s. Although no figures are presented, we also made the analysis for the cases when the spin polarization is directed along x and y, finding the maxima for $\hbar\omega = 0.088$ eV and $\alpha = 40°$, with $\mathcal{V}_{\sigma^x}(\omega,\alpha) = 37.4$ Km/s and $\mathcal{V}_{\sigma^y}(\omega,\alpha) = 24.8$ Km/s, $\gamma_x(\omega,\alpha) = 12.5°$, and $\gamma_y(\omega,\alpha) = 159.7°$

2. *alt structure*

We proceed to analyse the *alt* structure, just as we did the *up* structure. Fig. 6 shows $\mathcal{V}_{\sigma^z}(\omega,\alpha)$ (Eq. (13)), where we see that the maximum response is reached for $\hbar\omega = 0.912$ eV and a local maximum is obtained at $\hbar\omega = 0.720$ eV, both located in the short-wavelength infrared radiation (SWIR) range and for polarization angles, α, between 120° and 150°.

In Fig. 7 we plot $\mathcal{V}_{\sigma^z}(\omega,\alpha)$ vs. α (left scale,

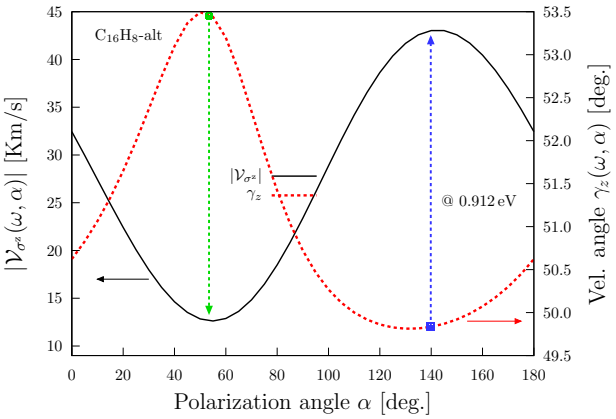

FIG. 7. Most intense response of $|\mathcal{V}_{\sigma^z}(\omega,\alpha)|$ (top frame, left scale) the corresponding velocity angle $\gamma_z(\omega)$ (top frame, right scale), the collinear (circled box) and perpendicular (square box) angles, and the two components $\mathcal{V}^{xz}(\omega)$ and $\mathcal{V}^{yz}(\omega)$ (bottom frame) for the *alt* structure fixing the energy to 0.912 eV. fig:alt-vaz-rag

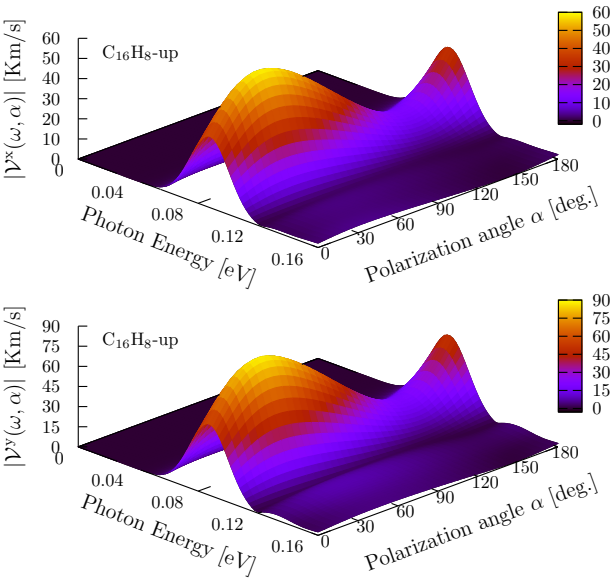

FIG. 8. $|\mathcal{V}^x(\omega,\alpha)|$ and $|\mathcal{V}^y(\omega,\alpha)|$responses as a function of the photon energy and polarization angle α for the *up* structure. The absolute maxima of both are localized in the energy range from 0.08 eV to 0.10 eV, in the Far Infrared, and for polarization angles from 25° to 50°. fig:up-3d-vva-1

black solid line), fixing the energy to 0.912 eV for which the response is maximized as shown in the top panel of Fig. 6. The absolute maximum is obtained for $\alpha = 145°$ with $\mathcal{V}_{\sigma^z}(\omega,\alpha) = 43.0$ Km/s. In the same panel we present the velocity angle $\gamma_z(\omega,\alpha)$ vs α (right scale, red dashed line), that for the absolute maximum is $\gamma_z(\omega,\alpha) = 49.9°$. Also, the green circle indicates the value of α for which the electrons move parallel to the incoming electric field, i.e. $\alpha = \gamma_z^{\parallel}(\omega,\alpha) = 53.5°$, with $\mathcal{V}_{\sigma^z}(\omega,\alpha) = 12.7$ Km/s. Likewise, the blue circle indicates the value of α for which the electrons move perpendicular to the incoming electric field, i.e. $\alpha = 140°$, with $\gamma_{z\perp}(\omega,\alpha) = 50°$, and $\mathcal{V}_{\sigma^z}(\omega,\alpha) = 43.0$ Km/s. We also have that $\gamma_z(\omega,\alpha)$ is centered at 51.5° having variations of ±2° for $0° \le \alpha \le 180°$. Again, for the cases in which the spin polarization is parallel to the surface the maximum values are $\mathcal{V}_{\sigma^x}(\omega,\alpha) = 27.1$ Km/s and $\mathcal{V}_{\sigma^y}(\omega,\alpha) = 33.2$ Km/s, corresponding to $\gamma_x(\omega,\alpha) = 100.1°$ $\gamma_y(\omega,\alpha) = 67.9°$ and both for $\alpha = 145°$, where the plots are not presented.

C. Fixing velocity

sec:res-fixvel

Using the Eq. (17), we calculated the $\mathcal{V}^a(\omega,\alpha)$ for the cases when the velocity is fixed along the a = x or a = y direction on the surface of the *up* and *alt* structures, and from the Eqns. (18) and (19), we determined the polar, $\theta_a(\omega,\alpha)$, and azimuthal, $\varphi_a(\omega,\alpha)$, angles corresponding to the direction of the spin.

1. *up structure*

In Fig. 8 we plot $\mathcal{V}^x(\omega,\alpha)$ and $\mathcal{V}^y(\omega,\alpha)$ for the *up* structure, where we see that each response has a maximum for $\hbar\omega = 0.088$ eV, in the LWIR, and $\alpha = 40°$. Fixing $\alpha = 40°$ eV, in Fig. 9 we plot $\mathcal{V}^x(\omega,\alpha)$ and $\mathcal{V}^y(\omega,\alpha)$ vs. $\hbar\omega$ (left scale, black solid line) where each responses has a maximum of 58.7 Km/s and 87.9 Km/s, respectively, for $\hbar\omega = 0.088$ eV. We also present the corresponding polar (right scale, red dashed line) and azimuthal (right scale, blue dashed line) spin polarization angles that have values of $\theta_x(\omega,\alpha) = 47.4°$, and $\varphi_x(\omega,\alpha) = 212.5°$ when the electron moves along x, and $\theta_y(\omega,\alpha) = 7.6°$, and $\varphi_y(\omega,\alpha) = 132.7°$, when the electron moves along y. This means that, the spin is directed upward the third Cartesian quadrant of the xy plane when the electron moves along x, and is directed almost perpendicularly over the xy plane

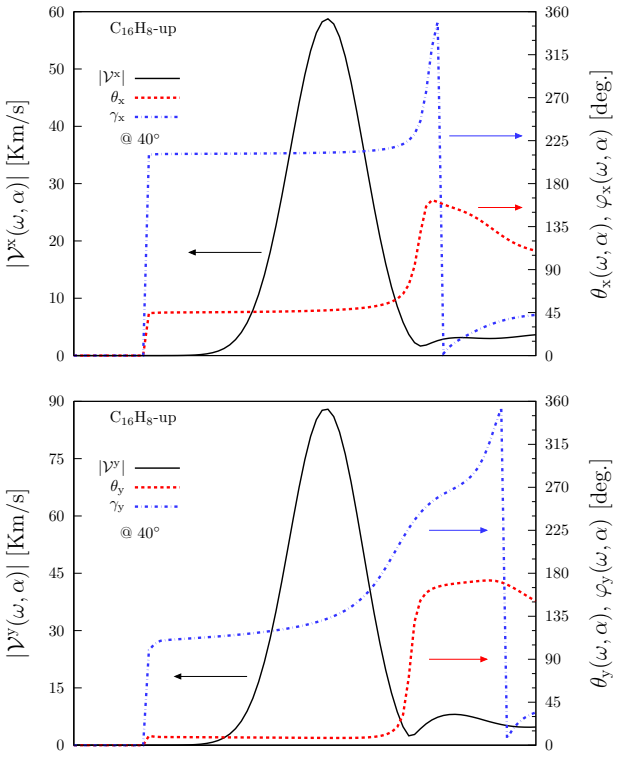

FIG. 9. Most intense response of $|\mathcal{V}^{\rm x}(\omega,\alpha)|$ and $|\mathcal{V}^{\rm y}(\omega,\alpha)|$ (top frames left scale of Figs. (a) and (b)), the corresponding polar φ and azimuthal θ angles (top frames right scale), and the corresponding three components (bottom frames) for the *up* structure fixing the polarization angle to $\alpha = 40°$ to maximize the response.

`fig:up-vab-comp-rtp-1`

when it moves along y. Also, from this figure we have that when the electron moves along x the spin direction is almost constant for all the energies across the peak of the response, having a ranges of $44.4° < \theta_{\rm x}(\omega,\alpha) < 56.2°$ and $210.3° < \varphi_{\rm x}(\omega,\alpha) < 217.4°$. Then, hen the electron moves along y the spin's polar angle has again minimal variations, $9.76° < \theta_{\rm y}(\omega,\alpha) < 13.7°$, but in contrast with this the azimuthal angle has significative variations, $99.3° < \varphi_{\rm y}(\omega,\alpha) < 196.1°$.

In Fig. 10, for the *up* structure, we plot $\mathcal{V}^{\rm a}(\omega,\alpha)$ vs. ω, and fixing $\alpha = 40°$; the range of ω lies in part of the VIS range. We see that there are two local maxima at $\hbar\omega = 1.932$ eV and $\hbar\omega = 1.972$ eV. For the latter that is the most intense we obtain $\mathcal{V}^{\rm x}(\omega,\alpha) = 9.9$ Km/s and $\mathcal{V}^{\rm y}(\omega,\alpha) = 49.4$ Km/s. For these local maxima, the corresponding polar and azimuthal spin polarization angles are $\theta_{\rm x}(\omega,\alpha) = 129.1°$, and

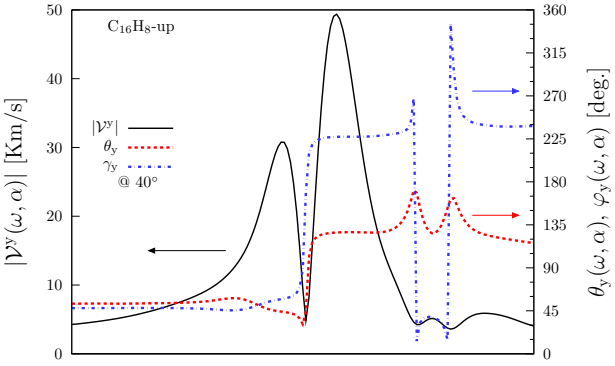

FIG. 10. Intense response of $|\mathcal{V}^{\rm x}(\omega,\alpha)|$ and $|\mathcal{V}^{\rm y}(\omega,\alpha)|$ (top frames left scale of Figs. (a) and (b)), the corresponding polar φ and azimuthal θ angles (top frames right scale), and the corresponding three components (bottom frames) for the *up* structure fixing the polarization angle to $\alpha = 40°$ to maximize the response.

`fig:up-vab-comp-rtp-2`

$\varphi_{\rm x}(\omega,\alpha) = 229.2°$, for the electron moving along x, and $\theta_{\rm y}(\omega,\alpha) = 127.0°$, and $\varphi_{\rm y}(\omega,\alpha) = 227.1°$ for the electron moving along y. We remark that these angles are almost constant for all the energy values across the peak of the this local maxima, for which the spin is directed downward in the third Cartesian quadrant of the xy plane when it moves along either x or y direc-

tions. For the $\hbar\omega = 1.932\,\text{eV}$ peak we obtain $\theta_{\text{x}}(\omega,\alpha) = 42.0°$, and $\varphi_{\text{x}}(\omega,\alpha) = 58.7°$, with $\mathcal{V}^{\text{x}}(\omega,\alpha) = 6.6$ Km/s, and $\theta_{\text{y}}(\omega,\alpha) = 45.2$, and $\varphi_{\text{y}}(\omega,\alpha) = 56.1$, with $\mathcal{V}^{\text{y}}(\omega,\alpha) = 29.0$ Km/s. However, for this local maximum, the spin angles are not constant across the resonant peak.

2. *alt structure*

In Fig. 11 we show for the *alt* structure $\mathcal{V}^{\text{x}}(\omega,\alpha)$ and $\mathcal{V}^{\text{y}}(\omega,\alpha)$ vs. ω, for $\alpha = 145°$, the value that maximizes both responses as a function of α, where we see that each response has two local maxima. The one at $\hbar\omega = 0.720$ eV gives $\mathcal{V}^{\text{x}}(\omega,\alpha) = 19.4??$ Km/s, and $\mathcal{V}^{\text{y}}(\omega,\alpha) = 51.9??$ Km/s, and the other one at $\hbar\omega = 0.912??$ eV gives $\mathcal{V}^{\text{x}}(\omega,\alpha) = 30.9$ Km/s and $\mathcal{V}^{\text{y}}(\omega,\alpha) = 52.3$ Km/s. For $\hbar\omega = 0.720$ eV, $\theta_{\text{x}}(\omega,\alpha) = 45.8°$, $\varphi_{\text{x}}(\omega,\alpha) = 40.7°$, $\theta_{\text{y}}(\omega,\alpha) = 140.7°$, and $\varphi_{\text{y}}(\omega,\alpha) = 221.6°$, implying that the spin is directed over the first Cartesian quadrant of the xy plane when the spin velocity is directed along x, and directed downward the third Cartesian quadrant when the spin velocity is directed along y. Finally, for $\hbar\omega = 0.912$ eV, $\theta_{\text{x}}(\omega,\alpha) = 153.8°$, $\varphi_{\text{x}}(\omega,\alpha) = 290.4°$, $\theta_{\text{y}}(\omega,\alpha) = 129.0°$, and $\varphi_{\text{y}}(\omega,\alpha) = 228.9°$, and the spin is directed downward in the fourth Cartesian quadrant of the xy plane when the spin velocity is directed along x and downward the third Cartesian quadrant when the spin velocity is directed along y.

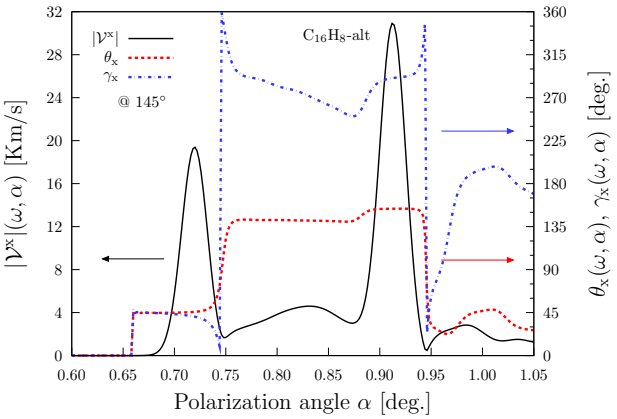

FIG. 11. Most intense response of $|\mathcal{V}^{\text{x}}(\omega,\alpha)|$ and $|\mathcal{V}^{\text{y}}(\omega,\alpha)|$ (top frames left scale of Figs. (a) and (b)), the corresponding polar φ and azimuthal θ angles (top frames right scale), and the corresponding three components (bottom frames) for the *alt* structure fixing the polarization angle to $\alpha = 145°$ to maximize the response. `fig:alt-vab-comp-rtp`

IV. CONCLUSIONS

`sec:conclusions`

We have performed an *ab initio* calculation for the SVI by one-photon absorption of linearly polarized light in the *up* and *alt* 2D hydrogenated graphene structures that and we made the calculation for the case when the spin is polarized in the z direction or when the velocity is directed along x or y; this effect does not seem to have been reported previously. This SVI is very sensitive to the symmetry characteristics of the structures presenting an anisotropic behavior. We found that the *up* structure has the most intense response resulting in $|\mathcal{V}_{\sigma^z}(\omega,\alpha)| = 95.8\,\text{Km/s}$ and $|\mathcal{V}^{\text{y}}(\omega,\alpha)| = 87.9\,\text{Km/s}$ for an energy of the incoming beam of $0.088\,\text{eV}$. Also the response of the *alt* structure is comparable to the response of GaAs and CdSe bulk semiconductors. The spin relaxation time in pure and doped graphene is long enough in the order from nanoseconds to milliseconds.[40,41] The, according to our results the *alt* structure is a good candi-

date and the *up* structure an excellent candidate for the development of spintronics devices that require PSC due to the high spin velocity transport. The fact that the *up* structure is better than the *alt* structure comes from the symmetry: the first one is *more* non-centrosymmetric than the second resulting in a more intense response of the system.

V. ACKNOWLEDGMENT

This work has been supported by *Consejo Nacional de Ciencia y Tecnología* (CONACyT), México, Grant No. 153930.

[1] S. A. Wolf, D. D. Awschalom, R. A. Buhrman, J. M. Daughton, S. Von Molnar, M. L. Roukes, A. Y. Chtchelkanova, and D. M. Treger, Science **294**, 1488 (2001).

[2] J. Fabian, A. Matos-Abiague, C. Ertler, P. Stano, and I. Zutic, Ac. Phys. Slov. (2007).

[3] D. D. Awschalom and M. E. Flatté, Nat. Phys. **3**, 153 (2007).

[4] S. Majumdar, R. Laiho, P. Laukkanen, I. J. Väyrynen, H. S. Majumdar, and R. Österbacka, App. Phys. Lett. **89**, 122114 (2006).

[5] S. Datta and B. Das, App. Phys. Lett. **56**, 665 (1990).

[6] M. Götte, M. Joppe, and T. Dahm, Scientific Reports **6** (2016).

[7] Y. V. Pershin and M. Di Ventra, Phys. Rev. B **78**, 113309 (2008).

[8] D. D. Awschalom, D. Loss, and N. Samarth, *Semiconductor Spintronics and Quantum Computation* (Springer Science & Business Media, 2013).

[9] S. Murakami, N. Nagaosa, and S. C. Zhang, Science **301**, 1348 (2003).

[10] A. Malshukov, C. Tang, C. Chu, and K.-A. Chao, Phys. Rev. B **68**, 233307 (2003).

[11] J. Sinova, D. Culcer, Q. Niu, N. A. Sinitsyn, T. Jungwirth, and A. H. MacDonald, Phys. Rev. Lett. **92**, 126603 (2004).

[12] R. D. R. Bhat and J. E. Sipe, Phys. Rev. Lett. **85**, 5432 (2000).

[13] A. Najmaie, R. D. R. Bhat, and J. E. Sipe, Phys. Rev. B **68**, 165348 (2003).

[14] R. D. R. Bhat, F. Nastos, A. Najmaie, and J. E. Sipe, Phys. Rev. Lett. **94**, 096603 (2005).

[15] H. Zhao, E. J. Loren, H. M. Van Driel, and A. L. Smirl, Phys. Rev. lett. **96**, 246601 (2006).

[16] M. J. Stevens, A. L. Smirl, R. D. R. Bhat, A. Najmaie, J. E. Sipe, and H. M. Van Driel, Phys. Rev. Lett. **90**, 136603 (2003).

[17] T. Kimura, N. Hashimoto, S. Yamada, M. Miyao, and K. Hamaya, NPG Asia Mat. **4**, e9 (2012).

[18] H. B. Heersche, P. Jarillo-Herrero, J. B. Oostinga, L. M. K. Vandersypen, and A. F. Morpurgo, Nature **446**, 56 (2007).

[19] A. Geim and K. Novoselov, Nat. Mater. **6**, 183 (2007).

[20] A. Reina, X. Jia, J. Ho, D. Nezich, H. Son, V. Bulovic, M. Dresselhaus, and J. Kong, Nano Lett. **9**, 30 (2008).

[21] K. S. Novoselov, Z. Jiang, Y. Zhang, S. V. Morozov, H. L. Stormer, U. Zeitler, J. C. Maan, G. S. Boebinger, P. Kim, and A. K. Geim, Science **315**, 1379 (2007).

[22] A. Balandin, S. Ghosh, W. Bao, I. Calizo, D. Teweldebrhan, F. Miao, and C. Lau, Nano Lett. **8**, 902 (2008).

[23] Y. Zhang, T. Tang, C. Girit, Z. Hao, M. Martin, A. Zettl, M. Crommie, Y. Shen, and F. Wang, Nature **459**, 820 (2009).

[24] M. Han, B. Özyilmaz, Y. Zhang, and P. Kim, Phys. Rev. Lett. **98**, 206805 (2007).

[25] Z. Ni, T. Yu, Y. Lu, Y. Wang, Y. P. Feng, and Z. Shen, ACS Nano **2**, 2301 (2008).

[26] D. Wei, Y. Liu, Y. Wang, H. Zhang, L. Huang, and G. Yu, Nano lett. **9**, 1752 (2009).

[27] B. Guo, L. Fang, B. Zhang, and J. R. Gong, Ins. J. **1**, 80 (2011).

[28] C. Coletti, C. Riedl, D. S. Lee, B. Krauss, L. Patthey, K. von Klitzing, J. H. Smet, and U. Starke, Phys. Rev. B **81**, 235401 (2010).

[29] A. Varykhalov, M. R. Scholz, T. K. Kim, and O. Rader, Phys. Rev. B **82**, 121101 (2010).

[30] D. C. Elias, R. R. Nair, T. M. G. Mohiuddin, S. V. Morozov, P. Blake, M. P. Halsall, A. C. Ferrari, D. W. Boukhvalov, M. I. Katsnelson, A. K. Geim, and K. S. Novoselov, Science **323**, 610 (2009).

[31] N. P. Guisinger, G. M. Rutter, J. N. Crain, P. N. First, and J. A. Stroscio, Nano Lett. **9**, 1462 (2009).

[32] D. K. Samarakoon and X. Q. Wang, ACS Nano **4**, 4126 (2010).

[33] R. Zapata-Peña, S. M. Anderson, B. S. Mendoza, and A. I. Shkrebtii, physica status solidi (b) **253**, 226 (2016).

[34] S. F. Alvarado, H. Riechert, and N. E. Christensen, Phys. Rev. Lett. **55**, 2716 (1985).

[35] B. Schmiedeskamp, B. Vogt, and U. Heinzmann, Phys. Rev. Lett. **60**, 651 (1988).
[36] F. Nastos, B. Olejnik, K. Schwarz, and J. E. Sipe, Phys. Rev. B **72**, 045223 (2005).
[37] X. Gonze, B. Amadon, P. M. Anglade, J. M. Beuken, F. Bottin, P. Boulanger, F. Bruneval, D. Caliste, R. Caracas, M. Côté, T. Deutsch, L. Genovese, P. Ghosez, M. Giantomassi, S. Goedecker, D. Hamann, P. Hermet, F. Jollet, G. Jomard, S. Leroux, M. Mancini, S. Mazevet, M. Oliveira, G. Onida, Y. Pouillon, T. Rangel, G.-M. Rignanese, D. Sangalli, R. Shaltaf, M. Torrent, M. Verstraete, G. Zerah, and J. Zwanziger, Comput. Phys. Commun. **180**, 2582 (2009).
[38] C. Hartwigsen, S. Goedecker, and J. Hutter, Phys. Rev. B **58**, 3641 (1998).
[39] F. Nastos, J. Rioux, M. Strimas-Mackey, B. S. Mendoza, and J. E. Sipe, Phys. Rev. B **76**, 205113 (2007).
[40] M. Wojtaszek, I. J. Vera-Marun, T. Maassen, and B. J. van Wees, Phys. Rev. B **87**, 081402 (2013).
[41] C. Ertler, S. Konschuh, M. Gmitra, and J. Fabian, Phys. Rev. B **80**, 041405 (2009).
LastBibItem